Heterogeneous & Homogeneous & Bio- & Nano-
CHEMCATCHEM
CATALYSIS

Accepted Article

Title: Effective Hydrogenolysis of Glycerol to 1,3-Propanediol over Metal-Acid Concerted Pt/WOx/Al2O3 Catalysts

Authors: Nian Lei, Xiaochen Zhao, Baolin Hou, Man Yang, Maoxiang Zhou, Fei Liu, Aiqin Wang, and Tao Zhang

To be cited as: *ChemCatChem* 10.1002/cctc.201900689

Link to VoR: http://dx.doi.org/10.1002/cctc.201900689

A Journal of
ChemPubSoc Europe

WILEY-VCH

www.chemcatchem.org

Effective Hydrogenolysis of Glycerol to 1,3-Propanediol over Metal-Acid Concerted $Pt/WO_x/Al_2O_3$ Catalysts

Nian Lei,[a,b] † Xiaochen Zhao,[a] † Baolin Hou,[a] Man Yang,[a,b] Maoxiang Zhou,[a,b] Fei Liu,[a] Aiqin Wang,*[a] Tao Zhang[a]

Abstract: Selective cleavage of secondary C-O bond is an important yet challenging strategy in glycerol valorization, and the product 1,3-propanediol (1,3-PDO) is of great value in polyester industry. Herein, we report a series of $Pt/WO_x/Al_2O_3$ catalysts for selective hydrogenolysis of glycerol in a fixed-bed reactor and obtain the highest space-time yield of 1,3-PDO ($191.7*10^{-3}$ $g_{1,3\text{-PDO}}$ h^{-1} $g^{-1}_{cat.}$) to date. Both Pt and W have substantial effects on the 1,3-PDO yield with the optimum Pt/W atomic ratio of 1/2~1/4. Spectroscopy characterizations as well as chemisorption experiments reveal that at the medium domain size of WO_x, hydrogen spillover can take place to the greatest extent due to the improved dispersion of Pt and the suitable reducibility of WO_x. Dehydration/dehydrogenation tests of 2-butanol suggest that strong Brønsted acid sites are created *via* hydrogen dissociation at the Pt-WO_x interface and spillover to the neighboring oxygen atom. Such in situ formed protons are critical to the selective cleavage of secondary C-O bonds of polyols.

Introduction

With the immense consumption of fossil resources, there are ever increasing concerns on the environmental issues such as greenhouse gas emissions and smoggy air. To alleviate the pressure on the environment, researchers are exploring the carbon-neutron biomass for the sustainable production of fuels and chemicals.[1] Glycerol, one of the top twelve biomass-derived platform molecules, is available at large scale and low cost as a byproduct in biodiesel production.[2] The valorization of glycerol is not only able to improve the economic competition of the biodiesel, but also able to contribute to the sustainability of the involved chemistry.[3-4]

Hydrogenolysis of glycerol to diols is one of the most important approaches to valorization.[5] The product selectivity is critically dependent on the catalyst composition and structure. For most transition metal catalysts supported on conventional oxides, such as Cu and Ru on silica,[6] the main product is 1,2-propanediol (1,2-PDO) as it is thermodynamically favorable.[7] In contrast to 1,2-PDO, 1,3-PDO is more valuable (5,000 $ vs. 2,000 $) and it is widely used as the monomer for production of PTT (polytrimethylene terephthalate), a high-quality polyester.[8] Therefore, the selective hydrogenolysis of glycerol to 1,3-PDO is highly desirable yet more challenging. Driven by the great potential for practical applications, this reaction has been intensively studied.[9-57] So far, it has been established that a noble metal in combination with an oxophilic metal oxide, typically like Ir-ReO_x[9-22], Rh-ReO_x[23-24] and Pt-WO_x[25-56], is effective for the formation of 1,3-PDO. In comparison with ReO_x, WO_x offers the advantage of better leaching-resistance and lower cost, therefore shows greater potential for practical applications. In an early report by Chaminand *et al.*,[25] it was found that the addition of tungstic acid to rhodium catalysts in a polar aprotic solvent sulfolane resulted in an increase of 1,3-PDO selectivity although the overall yield of 1,3-PDO was lower than 5%. Later, Kurosaka *et al.* improved the yield of 1,3-PDO to 24% by employing $Pt/WO_3/ZrO_2$ as the catalyst and DMI (1,3-dimethyl-2-imidazolidinone) as the solvent.[26] Similar to the $Pt/WO_3/ZrO_2$ catalyst, when Pt was deposited on sulfated zirconia, the resulting catalyst showed a high selectivity for 1,3-PDO in DMI solvent, and the 1,3-PDO yield reached as high as 55.6% after reaction at 170 °C and 7.3 MPa for 24 h.[57] However, in the above studies, organic solvents were used and played somehow a key role in the selectivity control.[58] From both economic and environmental point of view, water as the solvent would be highly desirable. When the reaction was carried out in aqueous phase, the hydrothermal stability of the catalyst must be considered. Zhu and coworkers studied the reaction in aqueous phase using a continuous fixed-bed reactor system. They initially used ZrO_2 supporting Pt-silicotungstic acid (HSiW) as the catalyst, and observed significant leaching of the HSiW species resulting in activity loss during the reaction. To improve the water tolerance of the catalyst, they then modified the catalyst with alkali metals and achieved good stability over Pt-LiSiW/ZrO_2 catalyst during 120 h time-on-stream meanwhile remaining high yield of 1,3-PDO (23.3 %).[27] In comparison with the water-soluble heteropolyacids, WO_3 is apparently more resistant to leaching. Qin *et al.* investigated the reaction over $Pt/WO_3/ZrO_2$ catalyst in a continuous fixed bed reactor system under mild reaction conditions (130 °C, 4 MPa H_2), and obtained 1,3-PDO yield of 32.0%.[28] However, using the same catalyst Gong *et al.* obtained an 1,3-PDO yield of only 6.3%.[29] Zhu *et al.* reported that the use of mixed oxides SiO_2-ZrO_2 could facilitate the dispersion of WO_3 and Pt and thus improved the activity and selectivity; the 1,3-PDO selectivity arrived at 52.0% at 54.3% conversion of glycerol.[30] Using $Pt/WO_3/TiO_2/SiO_2$ as the catalyst, Gong *et al.* obtained a high selectivity of 1,3-PDO (50.5% at 15.3 % glycerol conversion) after reaction at 180 °C and 5.5 MPa H_2 for 12 h, and they also found that the presence of TiO_2 was beneficial to the dispersion of Pt and WO_3.[31] In various oxide-supported Pt/WO_x catalyst systems, Pt/WO_x/AlOOH which

[a] Nian Lei, Xiaochen Zhao, Baolin Hou, Man Yang, Maoxiang Zhou, Fei Liu, Prof. Aiqin Wang, Prof. Tao Zhang
State Key Laboratory of Catalysis
Dalian Institute of Chemical Physics, Chinese Academy of Sciences
Dalian 116023, China
E-mail: aqwang@dicp.ac.cn
[b] Nian Lei, Man Yang, Maoxiang Zhou
University of Chinese Academy of Sciences
Beijing, 100049, China
† These authors contributed equally to this work.

Supporting information for this article is given *via* a link at the end of the document.

was first reported by Kaneda and coworkers,[32] appeared as the most promising one. Under the reaction condition of 180 °C, 5 MPa H_2 and 12 h, the selectivity of 1,3-PDO reached 66% with complete conversion of glycerol. The authors attributed the superior performance to the abundant hydroxyl groups of the boehmite support. However, the catalyst precursor was calcined at 800 °C prior to the reaction, which implied that the boehmite was probably transformed into γ-Al_2O_3 and that the hydroxyl groups on the surface might not be so important as the authors proposed. Following the work, García-Fernández *et al.* investigated the catalytic performance of Pt/WO_x/Al_2O_3 catalyst and obtained 1,3-PDO selectivity of 51.9% at 53.1% glycerol conversion when the Pt content was as high as 9 wt%.[33] Such a high content of Pt would make the catalyst very expensive and thereby limit the practical applications. Zhu *et al.* also investigated the catalytic performance of Pt/WO_x/Al_2O_3 using a continuous fixed-bed reactor system, and obtained 1,3-PDO yield of 42.4% when Pt and W contents were 2 wt% and 10 wt%, respectively.[34]

In spite of intensive studies, a clear image of the reaction mechanism as well as the exact active sites is still lacking. Tomishige and coworkers proposed that the reaction over the Ir-ReO_x proceeded *via* a direct hydride-proton mechanism by forming relatively stable 6-membered-ring intermediate at the interface of Ir-ReO_x.[10] Zhu *et al.* assumed that Brønsted acid sites on the support surface were responsible for the 1,3-PDO formation, while Lewis acid sites favored the 1,2-PDO formation.[34] However, that claim could not explain why glycerol was not converted at all in the absence of H_2 or Pt/Ir under otherwise identical conditions. Therefore, the discussion of acidity independently without concerning the contribution of noble metal species is unreasonable. In other words, the concert and balance between noble metal (Pt/Ir) and oxophilic oxides (WO_x/ReO_x) is paramount for the chemoselective hydrogenolysis.[59] However, the complexity in preparation and the close atomic numbers between the oxophilic element and noble metal render the structure identification rather challenging, thus limit the mechanistic understanding of supported Pt-W or Ir-Re catalysts as well as the rational design of catalysts.

In this contribution, we prepared a series of Pt/WO_x/Al_2O_3 catalysts and evaluated them for the selective hydrogenolysis of glycerol in a fixed-bed reactor and under relatively high glycerol concentration (50 wt%). Under the optimized Pt/W ratio and reaction conditions, we have obtained the highest 1,3-PDO productivity to date ($191.7*10^{-3}$ $g_{1,3\text{-PDO}}$ h^{-1} $g^{-1}_{cat.}$) over the 6Pt/12.9W/Al_2O_3 catalyst. By using various characterization techniques and dehydration/dehydrogenation of 2-butanol as the probe reactions, we have for the first time provided strong evidence that the in situ formed Brønsted acid sites *via* dissociation of H_2 at the Pt-WO_x interface and spillover of H atom to the WO_x surface were responsible for the high 1,3-PDO yield.

Results and Discussion

The series of Pt/WO_x/Al_2O_3 catalysts were evaluated for the hydrogenolysis of glycerol at a relatively high glycerol feed concentration (50 wt%), and the results are shown in Table 1. First, we investigated the effect of W loading at a constant Pt loading. When the Pt content was fixed at 2 wt%, both the glycerol conversion and the 1,3-PDO selectivity increased with the W loading, and the highest 1,3-PDO yield of 15.1% was obtained at the W loading of 7.5 wt%. Further increasing the W loading resulted in decrease of both glycerol conversion and 1,3-PDO selectivity. Similarly, when the Pt loading was kept at 4 wt%, increasing the W loading from 7.5 wt% to 12.9 wt% led to a remarkable increase of the glycerol conversion from 29.7% to 62.7%, together with a slight decrease of the 1,3-PDO selectivity. Further increasing the W loading to 20.4 wt% resulted in decline in both the glycerol conversion and 1,3-PDO selectivity. Clearly, the 1,3-PDO yield showed a volcano-shaped dependence on the W loading at each Pt content, and a higher W loading required a higher Pt loading to match it. On the other hand, when the W loading was fixed at 12.9 wt%, increasing the Pt loading from 1% to 6 wt% could bring about a proportional increase of the glycerol conversion, suggesting that the Pt dispersion remain constant within this range of Pt loading. However, further increase of the Pt loading to 8 wt% resulted in significant decrease of the glycerol conversion due to the decrease of the Pt dispersion. Meanwhile, the 1,3-PDO selectivity slightly decreased with an increase of the glycerol conversion, which was caused by the over-hydrogenolysis of glycerol to 1-PO. We also investigated the effect of Pt at other fixed W loadings, e.g., 7.5 % and 20.4 wt%, and observed similar trends. In terms of 1,3-PDO yield, the 6Pt/12.9W/Al_2O_3 was among the most active and selective catalysts, which afforded the 1,3-PDO yield of 28.4%.

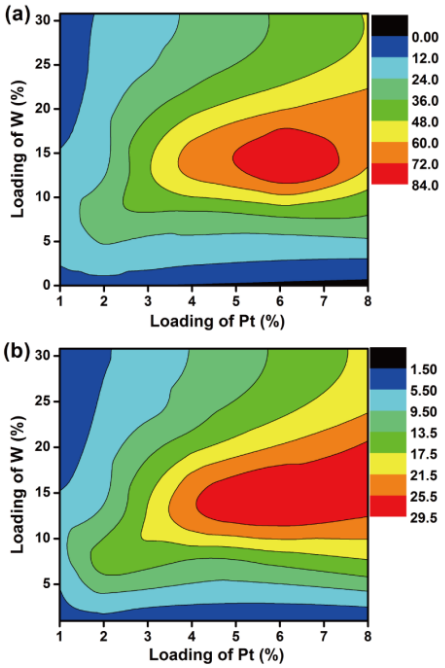

Figure 1. Contours showing the glycerol conversion (a) and 1,3-PDO yield (b) as functions of W and Pt loadings.

Table 1. Selective hydrogenolysis of glycerol over $Pt/WO_x/Al_2O_3$ catalysts.[a]

Entry	Catalyst	Conversion (%)	Selectivity (%)					1,3-PDO Yield (%)
			1,3-PDO	1,2-PDO	1-PO	2-PO	Others[b]	
1	$2Pt/Al_2O_3$	trace	0	100.0	0	0	0	0
2	$2Pt/1.0W/Al_2O_3$	10.8	37.7	22.9	23.4	5.9	10.1	4.1
3	$2Pt/4.0W/Al_2O_3$	22.2	42.8	13.3	24.6	7.7	11.5	9.5
4	$1Pt/7.5W/Al_2O_3$	15.9	46.2	14.0	25.9	8.0	5.9	7.3
5	$2Pt/7.5W/Al_2O_3$	31.2	48.5	9.9	29.6	10.7	1.3	15.1
6	$4Pt/7.5W/Al_2O_3$	29.7	43.5	10.0	28.0	10.1	8.4	12.9
7	$6Pt/7.5W/Al_2O_3$	34.0	43.3	9.5	29.8	9.9	7.5	14.7
8	$1Pt/12.9W/Al_2O_3$	14.6	44.1	17.2	24.8	10.3	3.6	7.0
9	$2Pt/12.9W/Al_2O_3$	22.9	44.8	16.8	26.0	10.3	2.1	10.2
10	$3Pt/12.9W/Al_2O_3$	46.5	38.3	13.1	31.7	11.1	5.8	17.8
11	$4Pt/12.9W/Al_2O_3$	62.7	39.4	9.8	36.3	12.2	2.3	24.7
12	$5Pt/12.9W/Al_2O_3$	70.1	39.5	7.2	38.9	13.0	1.4	27.7
13	$6Pt/12.9W/Al_2O_3$	80.4	35.3	4.9	41.8	12.3	5.7	28.4
14	$8Pt/12.9W/Al_2O_3$	57.7	43.5	7.0	35.5	11.5	2.5	26.1
15	$2Pt/20.4W/Al_2O_3$	20.1	38.0	13.4	29.6	10.3	8.7	7.6
16	$4Pt/20.4W/Al_2O_3$	43.1	36.2	10.4	33.7	10.9	8.8	15.6
17	$6Pt/20.4W/Al_2O_3$	57.2	37.3	8.9	35.6	11.6	6.6	21.3
18	$2Pt/30.8W/Al_2O_3$	13.4	38.1	14.6	35.6	9.7	2.0	5.1

[a] Reaction conditions: 180 °C, H_2 (5.0 MPa), 50 wt% GLY, GHSV = 1000 h^{-1}, LHSV = 1.0 h^{-1}.
[b] Others include propane, ethylene glycol, ethanol, methanol, methane and ethane.

Based on the data in Table 1, one can see that the effects of Pt and W loadings on the selective hydrogenolysis of glycerol to 1,3-PDO are interdependent, which can be illustrated as contours in Fig. 1. Considering both the yield of 1,3-PDO and the cost of catalyst, moderate Pt loading (e.g., 5 wt%) and medium W loadings (10~15 wt%) are favorable, and the suitable Pt/W atomic ratio is in the range of 1/2~1/4.

In addition to the catalyst composition, the reaction conditions also imposed impacts on the glycerol conversion and 1,3-PDO selectivity. As shown in Fig. S1, the glycerol conversion monotonically increased with the reaction temperature and hydrogen pressure, whereas the 1,3-PDO selectivity decreased dramatically with the rise of temperature due to over-hydrogenolysis to 1-PO, suggesting that lower temperature favors the formation of 1,3-PDO. Differently, the hydrogen pressure showed a positive effect on the 1,3-PDO yield. Liquid hourly space velocity (LHSV) and gas hourly space velocity (GHSV) were also investigated. Following the general feature of consecutive reactions, higher LHSV favored 1,3-PDO selectivity but caused decrease of the glycerol conversion. On the other hand, GHSV in the range of 1000~4000 h^{-1} had a negligible effect on the catalyst performance, suggesting that gas to liquid mass transfer was no longer a limiting factor when the GHSV was larger than 1000 h^{-1}.

Under the optimized reaction conditions, the highest space-time yield of 1,3-PDO ($191.7*10^{-3}$ h^{-1}) reported so far in the fixed-bed reaction systems (Table S1) was achieved, almost three times of the second best catalyst Ce-$Pt/WO_3/TiO_2$-SiO_2 ($69.0*10^{-3}$ h^{-1}).[60] When counting batch catalytic systems into comparison, the performance of the $6Pt/12.9W/Al_2O_3$ catalyst is still distinguished and next only to the Ir-ReO_x/SiO_2 catalyst,[9] whose component may be easily leached and hence unfeasible in fixed-bed reactor systems.

In order to understand the interdependent effects of Pt and W loadings on the catalyst performance and further to establish the structure-performance relationship, we conducted extensive characterizations of the series of $Pt/WO_x/Al_2O_3$ catalysts.

Fig. 2 shows XRD patterns of the series of $Pt/WO_x/Al_2O_3$ catalysts. The crystalline WO_3 was not detected until the W loading was above 20.4 wt% (Fig. 2a), indicating that the WO_x species were dispersed as sub-monolayer when its loadings on the Al_2O_3 support were below 20.4 wt%. In good agreement with the XRD results, the v (O–W–O) modes (714 cm^{-1} and 807 cm^{-1}) which were assigned to bridging oxygen of WO_6 octahedra,[61] appeared only when the W loading was above 20.4 wt% in the Raman spectra (Fig. 3a). In contrast, only the stretching mode of the distorted terminal W=O bond (959~989 cm^{-1}) was observed on the samples with W loading below 20.4 wt%. Moreover, this W=O vibration band shifted to lower wavenumbers and was broadened with reduction of the W loadings, suggesting the enhanced interaction of WO_x with Al_2O_3 surface and its decreased particle size.[62] Therefore, high W loading (> 20.4%) catalysts are likely to demonstrate the characteristics of bulk WO_3; while low to medium W loading WO_x catalysts display

distinctive chemistry. On the other hand, obvious diffraction peak of Pt was observed on the 4Pt/7.5W/Al_2O_3, while it did not emerge until the Pt loading increased to 8 wt% when the W loading was 12.9 wt% (Fig. 2b). This result suggested that submonolayer polytungstates are favorable for Pt dispersion, which is consistent with the activity results (Table 1).

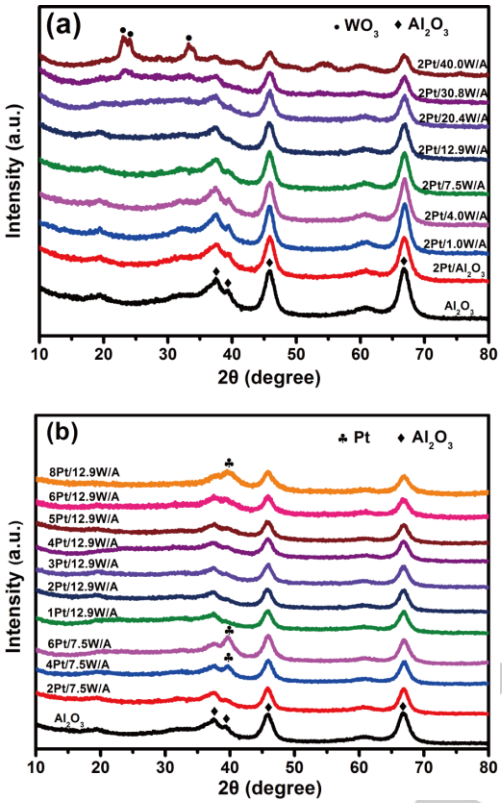

Figure 2. XRD patterns of the reduced Pt/Al_2O_3 and Pt/WO_x/Al_2O_3 catalysts with different W loading (a) and Pt loading (b).

Comparing the Raman spectra of WO_3/Al_2O_3 catalysts with and without platinum (Fig. 3a and 3b), one could see that the loading of Pt caused a shift of the vibrational band (W=O) from 959 cm^{-1} to 1004 cm^{-1}, accompanied by a slight increase in intensity. This shift of Raman band was supposed due to the interaction between platinum and surface tungsten oxides, resulting in the distortion of oxotungsten species.[63] It should be noted that the W=O band shift of Pt/WO_x/Al_2O_3 (1004 to 1024 cm^{-1}) followed the same trend as that of WO_3/Al_2O_3 (959 to 989 cm^{-1}) with the variation of W loadings, which suggests that the structure of the WO_x species is mainly determined by its surface density, irrespective of the loading of Pt.

To further clarify the structure of WO_x species, UV-vis, XPS, N_2 adsorption and ICP were conducted. In Fig. 4a, a gradual decrease of edge energy (E_g) with high transmittance was observed in the UV-vis diffuse reflectance spectra of WO_3/Al_2O_3, suggesting the electronic properties of WO_x substantially changed as the W loading increased. According to

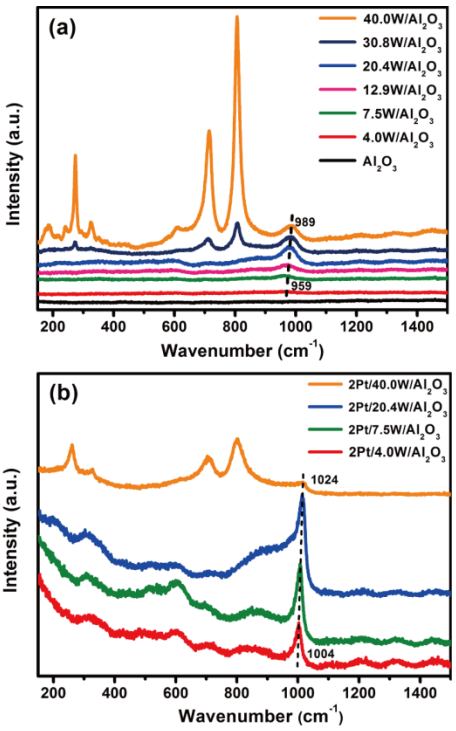

Figure 3. Raman spectra of the calcined WO_3/Al_2O_3 (a) and reduced Pt/WO_x/Al_2O_3 (b) catalysts.

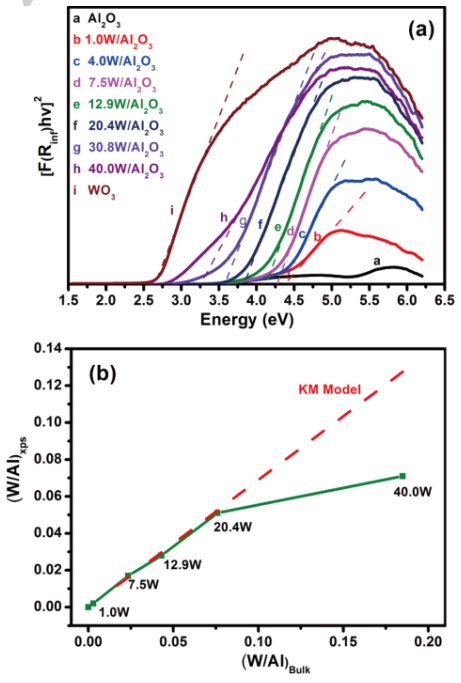

Figure 4. (a) Electronic edge values based on UV-vis spectra of the calcined WO_3/Al_2O_3 samples and (b) Surface atomic ratio ($(W/Al)_{XPS}$) as a function of bulk atomic ratio ($(W/Al)_{Bulk}$). The red dash line corresponds to Kerkhof-Moulijn model.

previous study[64] as well as XRD and Raman results, when the W loading was *ca.* 1-4 wt%, WO_x species were more likely to disperse as monotungstate (E_g > 4.4 eV) (Table 2). As the W loading was increased to 7.5 wt% and 12.9 wt%, both mono- and polytungstates coexitsted (4.4 eV > E_g > 4.0 eV). With a further increase of the W loading, the WO_x species consequently changed from polytungstates over the 20.4W/Al_2O_3 sample (E_g < 4.0 eV, W density < 4.5 W/nm^2 (monolayer W coverage)[65]) to 3D nanocluster WO_3 species over the 30.8W/Al_2O_3 and 40.0W/Al_2O_3 samples. This could be further validated by the Kerkhof-Moulijn (K-M) model in Fig. 4b. At W loading > 20.4 wt%, a deviation from monolayer deposition occurred.[66] It could thus be concluded that the sub-monolayer WO_x was formed on the Al_2O_3 surface when the W loading was below 20.4 wt%. It is noted that this threshold is much higher than that earlier reported (9 wt%).[33] The higher threshold obtained in this work might be due to the vacuum impregnation procedure as well as the favorable textural properties of the Al_2O_3 support.

Table 2. Structure identification of WO_3 in different WO_3/Al_2O_3 samples.

Sample	*Eg* (eV)	SA_{BET} (m^2g^{-1})	W density (W/nm^2)	Structure of W species
1.0W/Al_2O_3	4.4	185.7	0.2	monotungstate
4.0W/Al_2O_3	4.4	190.2	0.7	
7.5W/Al_2O_3	4.3	187.9	1.3	combination of mono- and polytungstates
12.9W/Al_2O_3	4.1	190.1	2.2	
20.4W/Al_2O_3	3.8	168.6	4.0	polytungstates
30.8W/Al_2O_3	3.6	150.1	6.7	nanocluster
40.0W/Al_2O_3	3.3	135.8	9.8	

As illustrated in Fig. 1, volcano profiles of glycerol conversion and 1,3-PDO yield were obtained as functions of both W and Pt loadings, and the optimized glycerol yield (~ 29%) could be obtained when Pt loading was *ca.* 5.0~7.0 wt% and W loading was *ca.* 11.0~17.0 wt% (1.9~2.9 W/nm^2), although with a little deviation. At this point, on the premise of highly dispersed Pt species, when monotungstate and polytungstates coexisted, the highest 1,3-PDO yield could be obtained.

The chemisorption of CO and H_2 was conducted on the series of Pt/WO_x/Al_2O_3 catalysts with a constant Pt loading of 2 wt% and various W loadings. As shown in Table 3, the CO uptakes increased only slightly when the W loading increased from 1 wt% to 12.9 wt%, correspondingly, the dispersion of Pt was slightly enhanced from 50.1% to 55.2%, which was close to that of Pt/Al_2O_3. However, at a higher W loading (≥ 20.4 wt%), the Pt dispersion was dramatically decreased to around 10%. This result indicated that the Al_2O_3-supported 2D sub-monolayer WO_x was beneficial to the Pt dispersion, while monolayer or 3D WO_x cluster led to strong interaction with Pt and partially covering the Pt sites upon H_2-reduction, which eventually caused dramatic decrease of CO uptakes. The mean particle size estimated from STEM was markedly smaller than that estimated from CO chemisorption for the high-W loading samples, approving that the Pt surface was overcoated with WO_x in these sample. The similar phenomenon was also observed on Pt/WO_x/TiO_2 catalysts.[67] The H_2 uptakes followed the same trend with CO chemisorption, however, the dispersion of Pt based on H_2 chemisorption was significantly higher than that based on CO chemisorption, indicating that hydrogen spillover occurred on the Pt/WO_x/Al_2O_3 catalysts.[67-69] Moreover, the degree of hydrogen spillover, which could be estimated from the difference between Pt dispersion^{CO} and Pt dispersion^{H_2}, was found to strongly depend on the interaction between Pt and WO_x and became the most pronounced on the 2Pt/7.5W/Al_2O_3 catalyst. Coincidently, this catalyst gave the highest 1,3-PDO yield among the series of catalysts.

Table 3. CO/H_2 chemisorption results of Pt/WO_x/Al_2O_3 catalysts.

Catalyst	Uptake (μmol/g)		Dispersion (%)		Particle size (nm)	
	CO	H_2	CO[a]	H_2[b]	d_{CO}[c]	d_{STEM}[d]
2Pt/Al_2O_3	57.2	32.3	55.8	63.0	2.0	1.6±0.4
2Pt/1.0W/Al_2O_3	51.4	31.0	50.1	60.5	2.3	1.2±0.3
2Pt/4.0W/Al_2O_3	52.6	37.7	51.3	73.5	2.2	--
2Pt/7.5W/Al_2O_3	53.4	44.3	52.1	86.4	2.2	1.1±0.4
2Pt/12.9W/Al_2O_3	56.6	34.2	55.2	66.7	2.0	--
2Pt/20.4W/Al_2O_3	16.4	19.6	16.0	38.2	7.1	1.7±0.4
2Pt/30.8W/Al_2O_3	10.4	9.7	10.1	18.9	11.1	--
2Pt/40.0W/Al_2O_3	7.7	5.9	7.5	11.5	15.0	2.3±0.7

[a] Determined by CO uptake based on CO/Pt = 1.
[b] Determined by H_2 uptake based on H_2/Pt = 2.
[c] Determined by the equation: d_{CO} = 1.13 / Dispersion^{CO}.[70]
[d] Determined by STEM.

Fig. 5 shows the HAADF-STEM images and particle size distributions. Among the four WO_3/Al_2O_3 samples, the 1.0W/Al_2O_3 sample (Fig. 5a) does not present any discernable nanoparticles, suggesting the WO_3 probably exists as isolated monomer.[71] On the other hand, both the 7.5W/Al_2O_3 and 20.4W/Al_2O_3 samples show highly dispersed WO_3 domains (Fig. 5c, e), and the poor contrast suggests the 2D structure of the WO_3 domains. In contrast, the obviously improved intensity of the WO_3 domains in the 40.0W/Al_2O_3 sample (Fig. 5g) strongly suggests that the WO_3 domains exist as 3D nanoparticles with an average size of 1.4 nm. This result is consistent with the above XRD, Raman, and UV-vis characterizations. After loading of Pt, the image contrast for low- to medium-W-loading catalysts (Fig. 5b, d) became much improved although the average particle sizes did not change much. This result suggests that most of the Pt particles probably reside on the WO_3 domains rather than on the alumina support. For the high-W-loading catalysts (2Pt/20.4W/Al_2O_3 and 2Pt/40.0W/Al_2O_3), the average Pt particle sizes were still below 3 nm although some bigger particles were occasionally observed (Fig. 5f, h). Such small sizes of Pt do not accord with the rather low CO and H_2 uptakes on these two samples, corroborating that strong metal support interaction (SMSI) occurred during the reduction treatment, which caused the partial encapsulation of Pt particles by the WO_x species.[67-68] This was further verified by the XPS Pt 4d spectra, in which the intensity of surface Pt gradually decreased when the W loading was increased, indicating less exposed Pt species (Fig. S2).

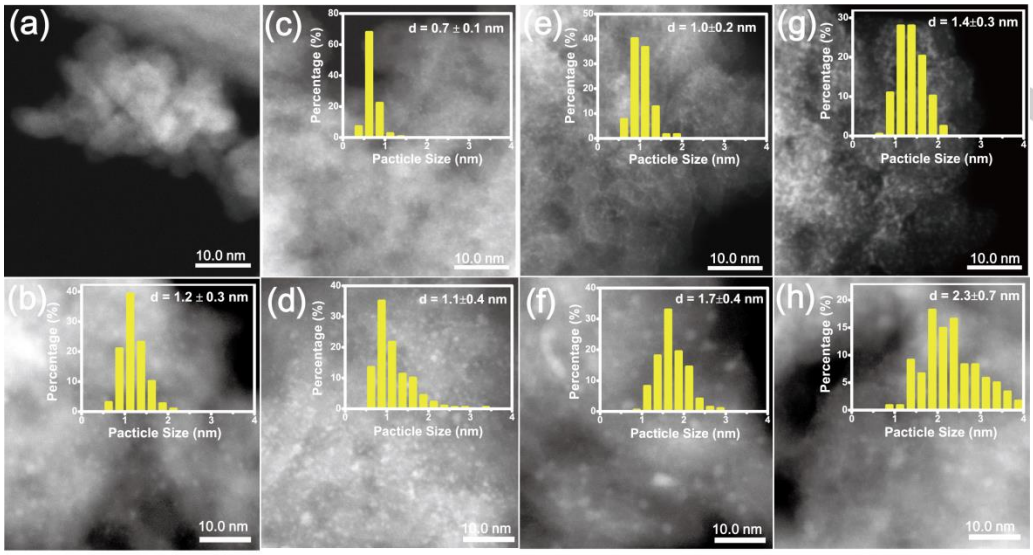

Figure 5. HAADF-STEM images of (a) 1.0W/Al_2O_3, (b) 2Pt/1.0W/Al_2O_3, (c) 7.5W/Al_2O_3, (d) 2Pt/7.5W/Al_2O_3, (e) 20.4W/Al_2O_3, (f) 2Pt/20.4W/Al_2O_3, (g) 40.0W/Al_2O_3, (h) 2Pt/40.0W/Al_2O_3.

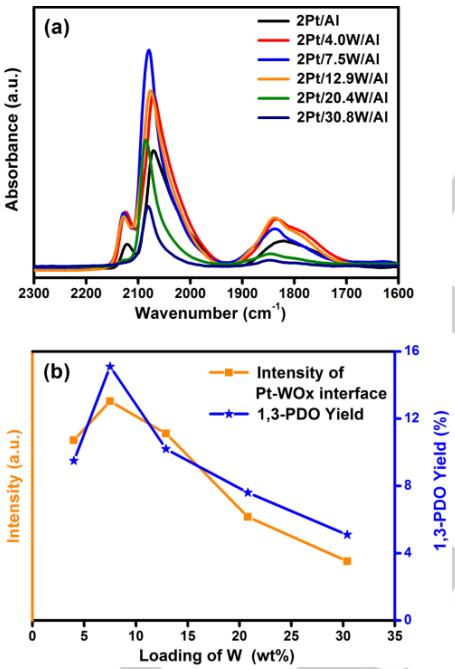

Figure 6. (a) DRIFT spectra of CO adsorbed on Pt/WO_x/Al_2O_3 catalysts and (b) the relationship between CO-adsorbed IR intensity at the Pt-WO_x interface and 1,3-PDO yield.

To further understand the interaction between Pt and WO_x, DRIFT spectra of adsorbed CO was performed to probe surface Pt sites with different W loadings. As shown in Fig. 6a, CO adsorption on the Pt/WO_x/Al_2O_3 catalysts produced three distinctive bands at 2122-2128 cm^{-1}, 2068-2085 cm^{-1} and 1829-1848 cm^{-1}. The band at 2122-2128 cm^{-1} can be ascribed to the CO adsorbed on isolated or positively charged Pt sites,[72-73] while the bands at 1829-1848 cm^{-1} are due to the CO bridgedly adsorbed on contiguous Pt sites.[74] On the other hand, the bands at 2068-2085 cm^{-1} are asymmetric and can be deconvoluted into three symmetric bands centred at 2070-2081 cm^{-1}, 2029-2049 cm^{-1} and 1986-2006 cm^{-1} (Fig. S3). The bands at 2070-2081 cm^{-1} can be assigned to CO adsorbed on Pt sites that are bonding with the WO_x domain (interfacial sites at the Pt-WO_x interface), while the latter two bands can be assigned to the typical linear adsorption of CO on Pt nanoparticles with different sizes.[75-76] It is interesting to note that with an increase of the W loading, the CO absorption band at the Pt-WO_x interface had a blue shift, indicating that electron transfer from Pt to W occurred. Moreover, the intensity of this band first increased with W loading and reached the highest at the 2Pt/7.5W/Al_2O_3 catalyst, then decreased with further increase of the W loading due to SMSI. We plotted the intensity of CO absorption band of each assignment as a function of W loading (Fig. S4) and found that only the CO adsorption at the Pt-WO_x interface changed in the same manner as the 1,3-PDO yield did, as shown in Fig. 6b. This result strongly suggests that the Pt-WO_x interfacial sites are catalytically active for the glycerol hydrogenolysis to 1,3-PDO.

In order to understand the key role of Pt-WO_x interface, we probed the origin of acidity for the glycerol hydrogenolysis. Firstly, we performed NH_3-TPD experiments to measure the permanent acid sites (not induced by H_2) on the catalyst surface. As shown in Fig. S5, the total amount of acid sites showed little difference from 2Pt/Al_2O_3 (0.63 mmol $NH_3/g_{cat.}$) to 2Pt/WO_x/Al_2O_3 (0.65-0.67 mmol $NH_3/g_{cat.}$) while the strong acid amount increased steadily with the W content. However, the negligible variance in the amount of permanent acids cannot account for the large difference in the 1,3-PDO yield, thus the contribution of the permanent acid sites on the WO_3/Al_2O_3 surface can be

precluded. Secondly, H_2SO_4 was introduced to the reaction system to investigate the role of aqueous Brønsted acids playing in the selective hydrogenolysis of glycerol. As shown in Table S2, both the glycerol conversion and the 1,3-PDO yield remained substantially unchanged when the feed pH was adjusted from 6.6 to 4.3 by introduction of H_2SO_4, but they dramatically dropped at lower pH conditions. This control experiment confirmed that the introduction of strong liquid Brønsted acid did not lead to the un-negligible improvement in the 1,3-PDO yield.

Since neither the solid surface acid sites nor the liquid acids are responsible for the selective production of 1,3-PDO, the in-situ generated Brønsted acids by dissociation and spillover of H_2 should be considered as the main contributor. To approve this, we used dehydration/dehydrogenation of 2-butanol under H_2 and N_2 atmosphere as the probe reaction to investigate the acidity produced by the dissociation and spillover of H_2.[77-79] Because both dehydration and dehydrogenation reactions can occur depending on the acid/metal ratios, this reaction can also be used to probe the bifunctionality of the catalysts.

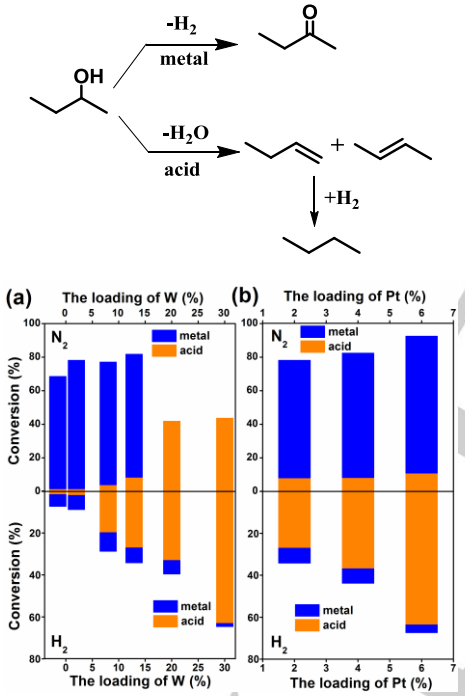

Figure 7. The conversion of 2-butanol in N_2 or H_2 over (a) $2Pt/WO_x/Al_2O_3$ catalysts with different W loading, and (b) $Pt/12.9W/Al_2O_3$ with different Pt loading.

As shown in Fig. 7, when the reaction was conducted in N_2, the $Pt/WO_x/Al_2O_3$ catalysts with the low to medium W loadings (< 20 wt%) mainly showed metallic nature by affording dehydrogenation products, irrespective of the Pt loading. The dehydrogenation activity can be well correlated with the CO chemisorption data (Fig. S6), showing its dependence on the exposed Pt sites. However, with an increase of the W loading, the dehydration product gradually appeared and eventually became predominant at the W loading greater than 20 wt%, indicating the acidity of the catalyst governed the reaction while the metallic nature was totally suppressed. This result is in good agreement with the DRIFTS, approving that higher W loading resulted in SMSI and significantly reduced the exposed Pt sites. On the other hand, when the reaction was conducted in H_2, the ratio of dehydration/dehydrogenation changed dramatically. Except for the $2Pt/Al_2O_3$ and $2Pt/4W/Al_2O_3$ both of which still showed dehydrogenation preference, all the other catalysts demonstrated dehydration preference. In particular, for the medium W loading catalysts (7.5 wt% W and 12.9 wt% W), the product selectivity was totally reversed by the presence of H_2, that is, dehydrogenation products predominated in N_2 while dehydration product dominated in H_2. Evidently, new acid sites were formed by the presence of H_2, possibly *via* hydrogen dissociation and then spillover of H atom to the interfacial WO_x species, in accordance with previous reports.[67] Consequently, the number of these new acid sites is critically dependent on the cooperation of Pt and WO_x, as revealed by the effect of Pt loading at fixed W loading of 12.9 wt% (Fig. 7b). In the presence of N_2, these series of catalysts all showed dehydrogenation capacities, whereas the presence of H_2 made them all be strongly acidic catalysts for the dehydration of 2-butanol, and the number of acid sites reached maximum at the $6Pt/12.9W/Al_2O_3$ catalyst. Coincidently, the best performance in terms of the 1,3-PDO was also achieved with the same catalyst, strongly suggesting that the newly created acid sites in the presence of H_2 were responsible for the selective hydrogenolysis of glycerol to 1,3-PDO.

Combining all the experimental and characterization results, we can postulate the reaction mechanism as below. The terminal OH of glycerol is protected by adsorption on WO_x[9-10, 33] while H_2 is activated and dissociated into two H atoms at the surface of Pt. Then, one H atom is spillover to the interfacial WO_3 site and reduce it to low-valence WO_x and concurrently form the Brønsted acid sites. When the polytungstates exist as 2D sub-monolayer with a medium domain size, the number of Pt-WO_x interface sites gets maximized due to highly dispersed Pt and appropriate reducibility of the WO_x, which favors the hydrogen spillover and promotes the in situ formation of strong Brønsted acid sites. The active protons then attack the secondary carbon of glycerol, forming the secondary carbocation intermediate, which could be hydrogenated by the Pt-H at the Pt-WO_x interface to form 1,3-PDO.

Conclusions

In summary, a series of $Pt/WO_x/Al_2O_3$ catalysts were prepared and evaluated for selective hydrogenolysis of glycerol to 1,3-PDO in the fixed-bed reactor and under a relatively high glycerol feed concentration. The catalytic performance was critically dependent on the cooperation between Pt and WO_x, and the highest 1,3-PDO productivity to date ($191.7*10^{-3}$ $g_{1,3\text{-PDO}}$ h^{-1} $g^{-1}_{cat.}$) has been obtained on the $6Pt/12.9W/Al_2O_3$ catalyst. Spectroscopy characterizations suggested that the reaction occurred at the Pt-WO_x interface, which could promote the in situ production of strong Brønsted acid sites through hydrogen

dissociation and spillover. The number of Pt-WO_x interfacial sites was maximized at the medium domain size of WO_x (7~15 wt% W) due to the appropriate electronic interaction with Pt. This mechanism understanding will help to guide the rational design of more efficient catalysts for the selective cleavage of secondary C-O bonds in a wide spectrum of biomass molecules, which is of importance for sustainable chemistry.

Experimental Section

Chemicals and materials

Glycerol, 1-propanol (1-PO), and 2-propanol (2-PO) were purchased from Tianjin Kemiou Chemical Reagent Co., Ltd. 1,2-propanediol (1,2-PDO) and n-butanol were purchased from Aladdin Chemistry Co., Ltd. 1,3-propanediol (1,3-PDO) was purchased from Acros chemicals co., Ltd. Al_2O_3 was synthesized and pelletized in our laboratory. Ammonium metatungstate (AMT) was purchased from Chenzhou Diamond Tungsten Products Co., Ltd. $H_2PtCl_6{\cdot}6H_2O$ was purchased from Tianjin Fengchuan Chemical Reagent technology Co., Ltd. 2-butanol was purchased from Sinopharm chemical reagent Co., Ltd.

Catalyst preparation

$Pt/WO_3/Al_2O_3$ catalysts were prepared by sequential impregnation method. Specifically, Al_2O_3 was vacuum impregnated with an aqueous solution of ammonium metatungstate (AMT), followed by drying at 110 ^oC for 12 h and calcination at 700 ^oC for 3 h to obtain a series of yWO_3/Al_2O_3 with different W contents (where y refers to the weight percent of W). Then, the yWO_3/Al_2O_3 samples were impregnated with an aqueous solution of $H_2PtCl_6{\cdot}6H_2O$, followed by drying at 110 ^oC for 12 h and calcination in static air at 300 ^oC for 3 h to obtain the $xPt/yWO_3/Al_2O_3$ catalyts (where x refers to the weight percent of Pt). For comparison, a Pt/Al_2O_3 sample was also prepared by the same procedure. The actual contents of W and Pt of the catalysts were measured by inductively coupled plasma atomic emission spectroscopy (ICP-AES). Prior to the XRD, STEM, Raman and XPS characterizations, all the $Pt/WO_x/Al_2O_3$ catalysts were reduced in flowing H_2 at 300 ^oC for 1 h, and passivated with 1% O_2/N_2 for 4 h at room temperature.

Catalyst characterization

Nitrogen adsorption-desorption measurements were performed at −196 ^oC on a Micromeritics ASAP 2460 instrument. The specific surface areas (S_{BET}) were calculated from the N_2 adsorption isotherm with BET equation, and the pore size distributions were obtained using desorption branch of the isotherms and BJH method. Prior to the physisorption measurements, the sample was firstly dehydrated at 110 ^oC for 1 h and then degassed at 300 ^oC for at least 4 h.

The power X-ray diffraction (XRD) patterns were acquired on a PW3040/60 X'Pert PRO (PANalytical) diffractometer equipped with a Cu Kα radiation source (λ= 0.15432 nm) operated at 40 kV and 40 mA. The X-ray patterns of reduced samples were collected in the 2θ range from 10° to 80°.

The Raman spectra were measured on a JobinYvon HR 800 Dispersive Raman Spectrometer with a resolution better than 2 cm^{-1}. The patterns of calcined and reduced samples were collected in the 150–1500 cm^{-1} regions.

HAADF-STEM images were obtained on a JEM-2100F Transmission Electron Microscope operated at 200 kV and equipped with EDS microanalysis system. The samples were prepared *via* ultrasonically dispersing the calcined or reduced powers into ethanol solvent and deposited on a holey C/Cu TEM grid.

UV–vis diffuse reflectance spectra (DRS) were obtained on a cintra (GBC) apparatus equipped with an integrated sphere attachment with $BaSO_4$ as the reference. The samples were loaded into a sample cell and measured in the region of 200–800 nm.

CO chemisorption, H_2 chemisorption, and Temperature-programmed desorption of NH_3 (NH_3-TPD) were conducted on a Micromeritics AutoChem II 2920 chemisorber. Prior to CO and H_2 chemisorption measurements, all the samples were pre-reduced at 300 ^oC under a stream of pure H_2 for 1 h, and then purged under inert gas (He for CO chemisorption and Ar for H_2 chemisorption) flow for 30 min at 310 ^oC. After being cooled down to 50 ^oC, pulses of 5% CO/He or 10% H_2/Ar were introduced to the reactor for CO or H_2 chemisorption until saturation was reached. The consumed CO or H_2 were detected with TCD and the uptakes were calculated by calibration with the standard sample.

In NH_3-TPD measurement, the samples were pre-reduced at 300 ^oC under a stream of pure H_2 for 1 h, and then purged under He flow at 310 ^oC for 30 min. After that, the samples were cooled down to 100 ^oC for NH_3 adsorption. After adsorption saturation, the samples were heated from 100 ^oC to 700 ^oC in He flow at a heating rate of 10 ^oC/min, while the desorbed NH_3 was monitored by a mass spectrometer system. In the measurement, m/e = 16 was monitored to analyze the desorbed NH_3 to avoid the interference of water.

The X-ray photoelectron spectra (XPS) of reduced samples were obtained on an ESCALAB 250 X-ray photoelectron spectrometer equipped with monochromated Al Kα anode. All binding energies were calibrated by referencing them to the energy of the C1s peak at 284.6 eV.

Diffuse reflectance infrared Fourier transform spectra (DRIFTS) were recorded with a Bruker Equinox 55 spectrometer equipped with a mercury cadmium telluride (MCT) detector at a resolution of 4 cm^{-1} using 128 scans. The sample was put into a cell, reduced at 300 ^oC under a stream of pure H_2 for 1 h and purged under He flow for 30 min at 310 ^oC. After cooled down to 50 ^oC, background spectrum was recorded. After that, 5% CO/He was introduced into the sample for 30 min. Pure He was subsequently introduced to the cell to remove the physically adsorbed CO, until the spectra of chemisorbed CO species were stable.

Glycerol hydrogenolysis

The hydrogenolysis of glycerol was carried out in a fixed-bed down-flow stainless steel reactor (length, 400 mm; internal diameter, 9.0 mm). The catalyst (2.0 mL, 20–40 mesh) was positioned between two beds of quartz sands. Prior to reaction, the catalyst was activated in flowing H_2 (120 mL/min) at 300 ^oC for 1 h. After cooling down the reactor to reaction temperature, aqueous solutions of glycerol were continuously pumped into the fixed-bed reactor through a high-pressure liquid pump. Hydrogen and glycerol solution flows were mixed at the inlet of the reactor. At the reactor outlet, the liquid and gas flows were cooled and separated in the gas-liquid separator. The standard reaction conditions were: 180 ^oC, 5.0 MPa, 50 wt% glycerol aqueous solution, GHSV = 1000 h^{-1}, LHSV = 1 h^{-1}. The effluent gas was analyzed online by Agilent 7890B GC with a HayeSep Q packed column (3 m ×1/8", TCD detector), while the liquid was off-line analyzed by the same GC with an HP-INNO WAX capillary column (30 m × 0.32 mm × 0.5 μm，FID detector) using n-butanol as

internal standard. The products were identified by GC–MS and confirmed with standard compounds, and the identified products included 1,3-propanediol (1,3-PDO), 1,2-propanediol (1,2-PDO), 1-propanol (1-PO), 2-propanol (2-PO), acetone, acetol, ethylene glycol, methanol, ethanol, propane, methane, ethane and CO_2. For all the reactions tested, the carbon balance was better than 97%. The conversion of glycerol and the selectivity of products were calculated after steady state was achieved (12 h time on stream, Fig. S7) based on the following equations:

Conversion of glycerol (%) = (mole of glycerol in – mole of glycerol out) / (mole of glycerol in)*100.

Selectivity (%) = (mole of carbon in specific product) / (mole of carbon in consumed glycerol)*100.

Dehydration/dehydrogenation tests of 2-butanol

The dehydration/dehydrogenation of 2-butanol was used as a model reaction to probe the acid sites of the catalysts. The reaction was conducted at 140 ^{o}C in a quartz flow reactor containing 0.050 g catalyst. Prior to the reaction tests, all the samples were reduced in flowing dry H_2 (20 mL/min) at 300 ^{o}C for 1 h. Liquid 2-butanol was bubbled with flowing H_2 or N_2 (20 mL/min) into the reaction system at 0.1 MPa and 60 ^{o}C. Reactant and product concentrations were measured by GC with an HP-INNO WAX capillary column (30 m × 0.32 mm × 0.5 μm，FID detector). In inert atmosphere, dehydration product (butene) and dehydrogenation product (butanone) were detected and verified by GC-MS; while in H_2 atmosphere, the dehydration product was further hydrogenated into butane.

Conversion of 2-butanol (%) = (mole of 2-butanol in – mole of 2-butanol out) / (mole of 2-butanol in)*100.

Selectivity (%) = (mole of specific product) / (mole of consumed 2-butanol)*100.

Acknowledgements

A. W. and T. Z. acknowledge the National Key Projects for Fundamental Research and Development of China (2018YFB1501600 and 2016YFA0202801), the National Natural Science Foundation of China (21690080, 21690084, 21721004, 21673228), the Strategic Priority Research Program of the Chinese Academy of Sciences (XDB17020100) and DICP ZZBS 201612 for financial supports.

Keywords: glycerol • hydrogenolysis • 1,3-propanediol • tungsten oxide • in situ acid sites

[1] M. Besson, P. Gallezot, C. Pinel, *Chem. Rev.* **2014**, *114*, 1827-1870.
[2] T. Werpy, G. Holladay, *Top Value Added Chemicals From Biomass Volume I-Results of Screening for Potential Candidates from Sugars and Synthesis Gas*, Department of Energy Washington DC, **2004**.
[3] M. Pagliaro, R. Ciriminna, H. Kimura, M. Rossi, C. Della Pina, *Angew. Chem., Int. Ed.* **2007**, *46*, 4434-4440.
[4] C. H. Zhou, J. N. Beltramini, Y. X. Fan, G. Q. Lu, *Chem. Soc. Rev.* **2008**, *37*, 527-549.
[5] D. Sun, Y. Yamada, S. Sato, W. Ueda, *Appl. Catal. B* **2016**, *193*, 75-92.
[6] Y. Wang, J. Zhou, X. Guo, *RSC Adv.* **2015**, *5*, 74611-74628.
[7] J. ten Dam, U. Hanefeld, *ChemSusChem* **2011**, *4*, 1017-1034.
[8] K. Tomishige, Y. Nakagawa, M. Tamura, *Green Chem.* **2017**, *19*, 2876-2924.
[9] Y. Nakagawa, Y. Shinmi, S. Koso, K. Tomishige, *J. Catal.* **2010**, *272*, 191-194.
[10] Y. Amada, Y. Shinmi, S. Koso, T. Kubota, Y. Nakagawa, K. Tomishige, *Appl. Catal. B* **2011**, *105*, 117-127.
[11] Y. Nakagawa, X. Ning, Y. Amada, K. Tomishige, *Appl. Catal. A* **2012**, *433-434*, 128-134.
[12] Y. Amada, H. Watanabe, M. Tamura, Y. Nakagawa, K. Okumura, K. Tomishige, *J. Phys. Chem. C* **2012**, *116*, 23503-23514.
[13] Y. Amada, H. Watanabe, Y. Hirai, Y. Kajikawa, Y. Nakagawa, K. Tomishige, *ChemSusChem* **2012**, *5*, 1991-1999.
[14] M. Tamura, Y. Amada, S. Liu, Z. Yuan, Y. Nakagawa, K. Tomishige, *J. Mol. Catal. A: Chem.* **2014**, *388-389*, 177-187.
[15] C. Deng, L. Leng, X. Duan, J. Zhou, X. Zhou, W. Yuan, *J. Mol. Catal. A: Chem.* **2015**, *410*, 81-88.
[16] C. Deng, L. Leng, J. Zhou, X. Zhou, W. Yuan, *Chin. J. Catal.* **2015**, *36*, 1750-1758.
[17] C. Deng, X. Duan, J. Zhou, X. Zhou, W. Yuan, S. L. Scott, *Catal. Sci. Technol.* **2015**, *5*, 1540-1547.
[18] W. Luo, Y. Lu, L. Gong, H. Du, M. Jiang, Y. Ding, *React. Kinet. Mech. Catal.* **2016**, *118*, 481-496.
[19] W. Luo, Y. Lu, L. Gong, H. Du, T. Wang, Y. Ding, *RSC Adv.* **2016**, *6*, 13600-13608.
[20] W. Luo, Y. Lu, L. Gong, H. Du, M. Jiang, Y. Ding, *Chin. J. Catal.* **2016**, *37*, 2009-2017.
[21] J. J. Varghese, L. Cao, C. Robertson, Y. Yang, L. F. Gladden, A. A. Lapkin, S. H. Mushrif, *ACS Catal.* **2019**, *9*, 485-503.
[22] Y. Nakagawa, M. Tamura, K. Tomishige, *Res. Chem. Intermed.* **2018**, *44*, 3879-3903.
[23] A. Shimao, S. Koso, N. Ueda, Y. Shinmi, I. Furikado, K. Tomishige, *Chem. Lett.* **2009**, *38*, 540-541.
[24] Y. Shinmi, S. Koso, T. Kubota, Y. Nakagawa, K. Tomishige, *Appl. Catal. B* **2010**, *94*, 318-326.
[25] J. Chaminand, L. a. Djakovitch, P. Gallezot, P. Marion, C. Pinel, C. Rosier, *Green Chem.* **2004**, *6*, 359-361.
[26] T. Kurosaka, H. Maruyama, I. Naribayashi, Y. Sasaki, *Catal. Commun.* **2008**, *9*, 1360-1363.
[27] S. Zhu, X. Gao, Y. Zhu, Y. Zhu, X. Xiang, C. Hu, Y. Li, *Appl. Catal. B* **2013**, *140-141*, 60-67.
[28] L. Qin, M. Song, C. Chen, *Green Chem.* **2010**, *12*, 1466-1472.
[29] L. Gong, L. Yuan, Y. Ding, R. Lin, L. I. Jingwei, W. Dong, W. Tao, W. Chen, *Chin. J. Catal.* **2009**, *30*, 1189-1191.
[30] S. Zhu, X. Gao, Y. Zhu, J. Cui, H. Zheng, Y. Li, *Appl. Catal. B* **2014**, *158-159*, 391-399.
[31] L. Gong, Y. Lu, Y. Ding, R. Lin, J. Li, W. Dong, T. Wang, W. Chen, *Appl. Catal. A* **2010**, *390*, 119-126.
[32] R. Arundhathi, T. Mizugaki, T. Mitsudome, K. Jitsukawa, K. Kaneda, *ChemSusChem* **2013**, *6*, 1345-1347.
[33] S. García-Fernández, I. Gandarias, J. Requies, M. B. Güemez, S. Bennici, A. Auroux, P. L. Arias, *J. Catal.* **2015**, *323*, 65-75.
[34] S. Zhu, X. Gao, Y. Zhu, Y. Li, *J. Mol. Catal. A: Chem.* **2015**, *398*, 391-398.
[35] S. Zhu, Y. Zhu, S. Hao, L. Chen, B. Zhang, Y. Li, *Catal. Lett.* **2011**, *142*, 267-274.
[36] T. Mizugaki, T. Yamakawa, R. Arundhathi, T. Mitsudome, K. Jitsukawa, K. Kaneda, *Chem. Lett.* **2012**, *41*, 1720-1722.
[37] S. S. Priya, V. P. Kumar, M. L. Kantam, S. K. Bhargava, A. Srikanth, K. V. R. Chary, *Ind. Eng. Chem. Res.* **2015**, *54*, 9104-9115.
[38] Q. Tong, A. Zong, W. Gong, L. Yu, Y. Fan, *RSC Adv.* **2016**, *6*, 86663-86672.
[39] T. Aihara, H. Kobayashi, S. Feng, H. Miura, T. Shishido, *Chem. Lett.* **2017**, *46*, 1497-1500.
[40] S. Garcia-Fernandez, I. Gandarias, Y. Tejido-Nunez, J. Requies, P. L. Arias, *ChemCatChem* **2017**, *9*, 4508-4519.
[41] S. García-Fernández, I. Gandarias, J. Requies, F. Soulimani, P. L. Arias, B. M. Weckhuysen, *Appl. Catal. B* **2017**, *204*, 260-272.
[42] Y. Fan, S. Cheng, H. Wang, D. Ye, S. Xie, Y. Pei, H. Hu, W. Hua, Z. H. Li, M. Qiao, B. Zong, *Green Chem.* **2017**, *19*, 2174-2183.
[43] Y. Fan, S. Cheng, H. Wang, J. Tian, S. Xie, Y. Pei, M. Qiao, B. Zong, *Appl. Catal. B* **2017**, *217*, 331-341.
[44] M. Edake, M. Dalil, M. J. D. Mahboub, J. L. Dubois, G. S. Patience, *RSC Adv.* **2017**, *7*, 3853-3860.
[45] S. Feng, B. Zhao, L. Liu, J. Dong, *Ind. Eng. Chem. Res.* **2017**, *56*, 11065-11074.
[46] G. Shi, Z. Cao, J. Xu, K. Jin, Y. Bao, S. Xu, *Catal. Lett.* **2018**, *148*, 2304-2314.
[47] G. Shi, J. Xu, Z. Song, Z. Cao, K. Jin, S. Xu, X. Yan, *Mol. Catal.* **2018**, *456*, 22-30.
[48] W. Zhou, Y. Zhao, Y. Wang, S. Wang, X. Ma, *ChemCatChem* **2016**, *8*, 3663-3671.
[49] W. Zhou, Y. Zhao, S. Wang, X. Ma, *Catal. Today* **2017**, *298*, 2-8.
[50] W. Zhou, J. Luo, Y. Wang, J. Liu, Y. Zhao, S. Wang, X. Ma, *Appl. Catal. B* **2019**, *242*, 410-421.
[51] L. Liu, Y. Zhang, A. Wang, T. Zhang, *Chin. J. Catal.* **2012**, *33*, 1257-1261.
[52] Y. Zhang, X. Zhao, Y. Wang, L. Zhou, J. Zhang, J. Wang, A. Wang, T. Zhang, *J. Mater. Chem. A* **2013**, *1*, 3724.

[53] J. Wang, N. Lei, C. Yang, Y. Su, X. Zhao, A. Wang, *Chin. J. Catal.* **2016**, *37*, 1513-1519.
[54] J. Wang, X. Zhao, N. Lei, L. Li, L. Zhang, S. Xu, S. Miao, X. Pan, A. Wang, T. Zhang, *ChemSusChem* **2016**, *9*, 784-790.
[55] X. Zhao, J. Wang, M. Yang, N. Lei, L. Li, B. Hou, S. Miao, X. Pan, A. Wang, T. Zhang, *ChemSusChem* **2017**, *10*, 819-824.
[56] S. Feng, B. Zhao, Y. Liang, L. Liu, J. Dong, *Ind. Eng. Chem. Res.* **2019**, *58*, 2661-2671.
[57] J. Oh, S. Dash, H. Lee, *Green Chem.* **2011**, *13*, 2004-2007.
[58] Y. Nakagawa, K. Tomishige, *Catal. Sci. Technol.* **2011**, *1*, 179-190.
[59] Y. Nakagawa, M. Tamura, K. Tomishige, *J. Mater. Chem. A* **2014**, *2*, 6688-6702.
[60] L. Gong, PhD thesis, Study on the Bifunctional Catalyst for Glycerol Hydrogenolysis to 1,3-Propanediol, University of Chinese Academy of Sciences (Beijing), **2011**.
[61] David G. Barton, Max Shtein, Ryan D. Wilson, S. L. S. And, Enrique Iglesia, *J. Phys. Chem. B* **1999**, *103*, 630-640.
[62] S. Eibl, B. C. Gates, H. Knözinger, *Langmuir* **2001**, *17*, 107-115.
[63] M. N. Taylor, W. Zhou, T. Garcia, B. Solsona, A. F. Carley, C. J. Kiely, S. H. Taylor, *J. Catal.* **2012**, *285*, 103-114.
[64] R. M. And, I. E. Wachs, *J. Phys. Chem. C* **2007**, *111*, 15089-15099.
[65] I. E. Wachs, T. Kim, E. I. Ross, *Catal. Today* **2006**, *116*, 162-168.
[66] V. León, *Surf. Sci.* **1995**, *339*, 931–934.
[67] J. He, S. P. Burt, M. Ball, D. Zhao, I. Hermans, J. A. Dumesic, G. W. Huber, *ACS Catal.* **2018**, *8*, 1427-1439.
[68] J. G. Santiesteban, D. C. Calabro, W. S. Borghard, C. D. Chang, J. C. Vartuli, Y. P. Tsao, M. A. Natal-Santiago, R. D. Bastian, *J. Catal.* **1999**, *183*, 314-322.
[69] R. Prins, *Chem. Rev.* **2012**, *112*, 2714-2738.
[70] X. Chen, X. Su, H. Su, X. Liu, S. Miao, Y. Zhao, K. Sun, Y. Huang, T. Zhang, *ACS Catal.* **2017**, *7*, 4613-4620.
[71] W. Zhou, E. I. Ross-Medgaarden, W. V. Knowles, M. S. Wong, I. E. Wachs, C. J. Kiely, *Nat. Chem.* **2009**, *1*, 722-728.
[72] L. DeRita, S. Dai, K. Lopez-Zepeda, N. Pham, G. W. Graham, X. Pan, P. Christopher, *J. Am. Chem. Soc.* **2017**, *139*, 14150-14165.
[73] K. Ding, A. Gulec, A. M. Johnson, N. M. Schweitzer, G. D. Stucky, L. D. Marks, P. C. Stair, *Science* **2015**, *350*, 189-192.
[74] O. S. Alexeev, G. W. Graham, D. W. Kim, M. Shelef, B. C. Gates, *PCCP* **1999**, *1*, 5725-5733.
[75] P. Bazin, O. Saur, J. C. Lavalley, M. Daturi, G. Blanchard, *PCCP* **2005**, *7*, 187-194.
[76] M. J. Kale, P. Christopher, *ACS Catal.* **2016**, *6*, 5599-5609.
[77] C. D. Baertsch, K. T. Komala, Y.-H. Chua, E. Iglesia, *J. Catal.* **2002**, *205*, 44-57.
[78] J. Macht, C. D. Baertsch, M. May-Lozano, S. L. Soled, Y. Wang, E. Iglesia, *J. Catal.* **2004**, *227*, 479-491.
[79] D. Shi, H. Wang, L. Kovarik, F. Gao, C. Wan, J. Z. Hu, Y. Wang, *J. Catal.* **2018**, *363*, 1-8.

FULL PAPER

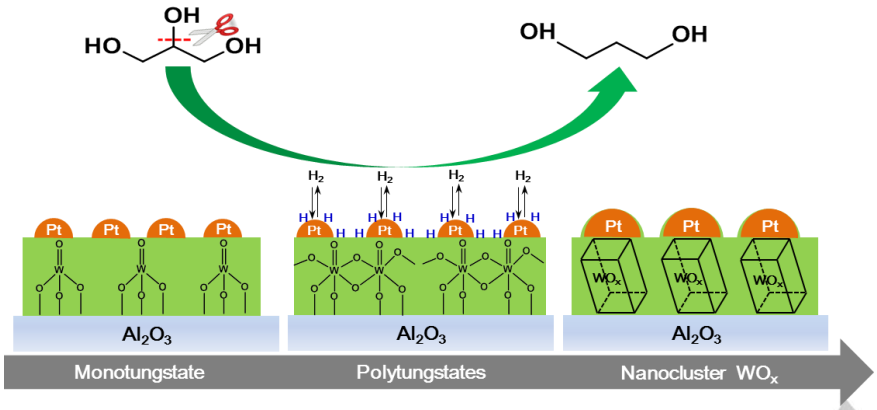

Nian Lei, Xiaochen Zhao, Baolin Hou, Man Yang, Maoxiang Zhou, Fei Liu, Aiqin Wang, and Tao Zhang*

Page 1. – Page 11.

Effective Hydrogenolysis of Glycerol to 1,3-Propanediol over Metal-Acid Concerted $Pt/WO_x/Al_2O_3$ Catalysts

The highest 1,3-PDO yield was obtained over the $Pt/WO_x/Al_2O_3$ catalyst with a medium domain size of WO_x and a Pt/W atomic ratio of 1/4~1/2, which favored the dispersion of Pt and maximized the number of Pt-WO_x interface sites, and consequently promoted the in-situ production of strong Brønsted acid sites.